applied sciences

MDPI

Article

Effect of TiO_2 Addition on Mortars: Characterization and Photoactivity

M. J. Hernández-Rodríguez [1,*], R. Santana Rodríguez [2], R. Darias [2], O. González Díaz [1], J. M. Pérez Luzardo [2], J. M. Doña Rodríguez [1] and E. Pulido Melián [1,*]

[1] Grupo de Fotocatálisis y Espectroscopia para Aplicaciones Medioambientales (FEAM, Unidad Asociada al CSIC), Dpto. de Química, Instituto de Estudios Ambientales y Recursos Naturales (i-UNAT), Universidad de Las Palmas de Gran Canaria, 35017 Las Palmas de Gran Canaria, Spain

[2] Departamento de Construcción Arquitectónica (Materiales Ecoestructurales), Universidad de Las Palmas de Gran Canaria, 35017 Las Palmas de Gran Canaria, Spain

* Correspondence: mariajosehr2@gmail.com (M.J.H.-R.); elisenda.pulido@ulpgc.es (E.P.M.)

Received: 10 May 2019; Accepted: 24 June 2019; Published: 27 June 2019

Abstract: In this study, mortar specimens were prepared with a cement:sand:water ratio of 1:3:0.5, in accordance with standard EN196-1. Portland CEM I 52.5 R grey (G) and white (W) cements were used, together with normalised sand and distilled water. Different amounts of TiO_2 photocatalyst were incorporated in the preparation of the mortar samples. The effect of the addition of TiO_2 was studied on mechanical properties of the mortar and cement including compressive and flexural strength, consistency (the flow table test), setting time and carbonation. Characterization techniques, including thermogravimetry, mercury porosimetry and X-ray diffraction spectroscopy (XRD), were applied to study the physico-chemical properties of the mortars. It was shown that adding the photocatalyst to the mortar had no negative effect on its properties and could be used to accelerate the setting process. Specimen photoactivity with the incorporated photocatalyst was tested for NOx oxidation in different conditions of humidity (0% RH and 65% RH) and illumination (Vis or Vis/UV), with the results showing an important activity even under Vis radiation.

Keywords: mortar; cement; TiO_2; NOx; photocatalysis

1. Introduction

As population levels have grown worldwide, so new problems have arisen for mankind to deal with, including high levels of pollutant emissions as the result of fossil fuel combustion. These harmful agents not only endanger human health and the environment but also lower the durability of concrete structures through acidification and degradation and consequently increase maintenance and restoration costs. According to European Commission data, atmospheric contamination causes 370,000 premature deaths each year in the European Union [1]. High levels of pollution in the air we breathe provoke cardio-respiratory problems (arrhythmias, asthma, bronchitis, allergies) [2]. Vehicular traffic is the main source of atmospheric emissions. The highest concentrations of air pollution tend to be found in urban environments, especially densely populated urban centres. The flat external surfaces of construction elements found in these urban centres are exposed to solar radiation and air contamination. Measures that can be adopted to improve air quality include greater use of public transport and the lowering of speed limits. One very recent method for air quality enhancement involves the use of photocatalytic products in elements used for urban construction. Previous studies have shown that these photocatalytic products are able to degrade a wide range of organic compounds (e.g., volatile organic compounds) and some inorganic compounds (NOx and SO_2), which are aggressive for both the materials and the environment [3–6].

The incorporation of photocatalysts in different construction materials was first conceived in Japan at the start of the 1990s [7]. Its use has extended to the rest of the world, notably accelerating in the last decade [8]. Photocatalytic performance in urban environments can be affected by environmental factors such as incident radiation intensity, relative humidity, temperature and wind, in addition to other intrinsic factors of the photocatalyst when this is associated to a cement-based support [9,10].

Though the effect of the photocatalytic decontamination of construction materials is clear, there remain a number of unresolved problems when using these materials in real applications [11]. There are presently various companies manufacturing photocatalytic cements and other materials for their application on facades, streets, pavements, roofs and so forth, with multiple examples of their application in Japan and Europe [12]. Though photocatalytic materials are now being marketed, many of the products have not been competitive or commercially successful. There is therefore a need to synthesise new photocatalytic materials and design strategies or methods for their incorporation in the binders and additives which form the basis of these materials. It is vital not only that the photocatalysts remain active despite the strongly alkaline matrix they are incorporated in but also that the construction materials continue to meet the legally required specifications in terms of mechanical properties.

An analysis is undertaken in this work of the incorporation of photocatalysts in mortars, studying the structural changes that take place in the photocatalytic mortars and their capacity for NOx elimination. The selected photocatalysts (Aeroxide TiO_2 P25 and Kronos vlp7000) are two of the commercial photocatalysts that have displayed the highest efficiency in the oxidation of NOx in published studies [13].

2. Materials and Methods

2.1. Elaboration of Specimens

In accordance with standard EN196-1, specimens of 40 mm·40 mm·160 mm were made. The blank specimens were made from one-part cement, three-parts normalised CEN EN196-1 sand (Instituto Eduardo Torroja) and half-part water (water/cement ratio = 0.5). Each mix for three specimens consisted of 450 g of cement, 1350 g of sand and 225 g of water. The cements, CEM I 52.5 R (white and grey), were supplied by CEISA (Cementos Especiales de las Islas S.A., Canary Islands, Spain), a local producer that fully meets the specifications determined by the European Union for this type of cement. Incorporation of the photocatalyst was carried out by replacing 5%wt. and 10%wt. of the cement. These percentages were chosen on the basis of Standard UNE-EN 934-2 which limits additive content in mortar to 5%wt. and Standard UNE-EN 12878:2014 which allows the addition of pigments of up to 10%wt. Specimens of the same dimensions were also prepared but with the catalyst only incorporated as part of the surface layer of the specimen. In these specimens, up to 50%wt. of catalyst was attained by increasing the water content in the preparation of the layer to a water/cement ratio = 1.3. For this, two mortar preparations were made at the same time: one with grey cement in which the TiO2 nanoparticles were not incorporated and another with white cement in which part of the cement was replaced with TiO2. The first of these preparations was deposited in the moulds to a height of 30 mm and the second preparation was then added to raise the height to 40 mm. The photocatalytic layer was made with white cement to avoid absorption of radiation by the non-active material, although it was subsequently found that this was not a determining factor with the radiation source that was employed. The catalysts used were the Aeroxide TiO_2 P25 (P25) catalyst, manufactured by Evonik Industries, and, in a subsequent study for purposes of comparison, the Kronos vlp7000 (Kronos) catalyst which has photocatalytic properties under visible radiation [14]. Titanium is an abundant element and ever more efficient extraction processes are being designed from both an economic and environmental point of view [15]. Distilled water was used throughout the experiments. The samples were respectively named W and G for the white and grey cement-based specimens with no added photocatalyst, W-5 and G-5 for the specimens with the incorporation of 5%wt. of photocatalyst and W-10 and G-10 for the

specimens with the incorporation of 10%wt. of photocatalyst. All tests were conducted in a specialist laboratory for construction materials in our research centre.

2.2. Photoactivity Tests

The photoactivity tests were performed using a similar system to the one extensively described in References [13] and [16]. The reactor allows the incorporation of 40 mm·40 mm·160 mm specimens in its interior with a 5 mm space in the upper part for the flow of gases. The reactor is equipped with an airtight borosilicate lid leaving a headspace between the lower face of the lid and the surface of the mortar specimen. The gas flow travelling through the empty reactor volume (0.32 mL) was of turbulent regime. Total input work flow was 1.2 L·min^{-1} at 1 atm and reactor residence time was 1.60 s. The concentration of NOx was obtained from dilution with air of a 100 ppm concentration of NO (supplied by Air Liquide) using mass flow controllers. The concentration for the experiments was 500 ppb NO ([NO_2] = 20 ± 5 ppb). For the addition of humidity, an extra air-pipeline was used which passed through a thermostatically controlled water bath. The light source employed was an Osram Ultra Vitalux 300 W lamp, situated 29 cm above the reactor. The temperature of the specimen increased from 24 °C to no more than 27 °C thanks to the use of air fans to dissipate the heat. The total incident light flux of this lamp in the range 300–430 nm is 1.54 × 10^{14} photons mol·cm^{-2}·s^{-1} (33.8% UV and 76.2% Vis). A Schott filter (cut-off wavelength 400 nm) was placed between the reactor and the lamp for the tests with visible light. NOx measurements were analysed with a Horiba APNA-370 N/S chemiluminescence monitor.

The results shown are the average of two tests with a maximum deviation of 5%. The results are expressed as percentages of $[NO]_{removed}$, $[NO_2]_{generated}$ and $[NOx]_{removed}$ in accordance with the following Equations:

$$NO_{removed}/\% = \int_{t_o}^{t} \frac{[NO]_{in} - [NO]_{out}}{[NO]_{in}} \cdot dt \cdot 100 \quad (1)$$

$$NO_{2generated}/\% = \int_{t_o}^{t} \frac{[NO_2]_{out} - [NO_2]_{in}}{[NO]_{in}} \cdot dt \cdot 100 \quad (2)$$

$$NO_{xremoved}/\% = \int_{t_o}^{t} \frac{([NO]_{in} + [NO_2]_{in}) - ([NO]_{out} + [NO_2]_{out})}{[NO]_{in}} \cdot dt \cdot 100 \quad (3)$$

where $[NO]_{in}$ and $[NO_2]_{in}$ are the concentrations after 30 min of adsorption and $[NO]_{out}$ and $[NO_2]_{out}$ are the concentrations at the end of the illumination period.

2.3. Characterisation Tests of Building Materials

The mortar was mechanically mixed and compacted in a mould with a compacter. The specimens were kept in the mould in a humid atmosphere (around 100%) for 24 h. After removal from the mould, the specimens were submerged in water for 28 days and then left exposed to the environmental conditions on the roof of the building (Campus de Tafira, Las Palmas de Gran Canaria, 28°04'49.7"N 15°27'08.8"W). The compression and flexural strength studies were performed in accordance with standard EN196-1 at 2 days, 7 days, 28 days, 90 days, 200 days and 365 days. Initial and final setting times were determined following standard EN196-3 and consistency following standard EN 1015-3. Sample carbonation was determined with a solution of phenolphthalein at 1% in ethanol at 28 days and 365 days. Pore distribution was measured by mercury intrusion porosimetry (MIP, Poremaster, Quantachrome Corp., USA). Specimen cylinders were extracted using a 12 mm diamond tipped bit, washed with isopropanol and oven-dried for 2 days at 105 °C. To obtain the X-ray diffractograms, a PANalytical X'Pert Pro system (PANalytical B.V., Netherlands, 2009) was used with Cu radiation (1.54 Å, 45 kV, 40 mA) and an X´Celerator detector measuring over 60 seconds per step in a range from

5° to 80°, with a step size of 0.02°. The differential heat analysis and thermogravimetric analysis were performed with a Netzsch STA 409/CD (N_2 at 80 mL·min^{-1}, 10 K·min^{-1}) system (Netzsch-Gerätebau GmbH, Germany, 2015), enabling determination of the percentages of hydration and of portlandite of the specimens.

3. Results

3.1. Mechanical properties

Though the mortars in our study are not specifically for masonry work, a study was nevertheless made of their consistency and the effect on consistency of adding the catalyst. No changes were observed in this respect with the addition of P25 to cements G and W, though it was noted that the mixtures were slightly drier, especially those of cement W. This is due to the specific surface area and shape index of the particles of the photocatalytic addition which have a higher water adsorption capacity in the open time of the mixture in workable state. The water vapour adsorption capacity for the P25 was found to be 0.35 mg·m^{-3}, which explains this phenomenon.

Table 1 and Figure 1 show the results of the flexural and compressive strength tests, respectively. As can be seen, all specimens display the same strength versus time pattern. The presence of the photocatalyst does not seem to produce any important alterations in terms of flexural strength in either cement W or G. Though there is an overall trend for flexural strength to decrease as the amount of catalyst is increased, this decrease is not significant. As for compression strength, a decrease can be seen with the incorporation of the TiO_2 catalyst in both the W and G cements, though without falling below the minimum value of 52.5 MPa established in the corresponding standards. The compression strength in the W series is slightly higher, both with and without the addition of the photocatalyst, than the corresponding values in the G series. The differences in compression strength between the cements without and with added catalyst are higher from 90 days onwards. Loss of resistance has also been observed by other authors with the incorporation of more than 1%wt. TiO_2 [17]. The decrease in strength is normally caused by an increase in porosity [18–20]. In our samples, an increase in porosity was also observed caused by the addition of TiO_2 nanoparticles, as will be shown later.

Table 1. Results of flexural strength tests (MPa).

days	G	G-5	G-10	W	W-5	W-10
2	6.33	6.13	5.61	6.42	6.08	6.06
28	9.05	8.21	8.29	8.65	8.70	7.53
90	10.40	9.41	9.41	9.95	9.61	8.88
200	11.20	9.86	9.81	10.32	10.18	10.28
365	12.26	11.20	10.91	12.01	10.69	10.32

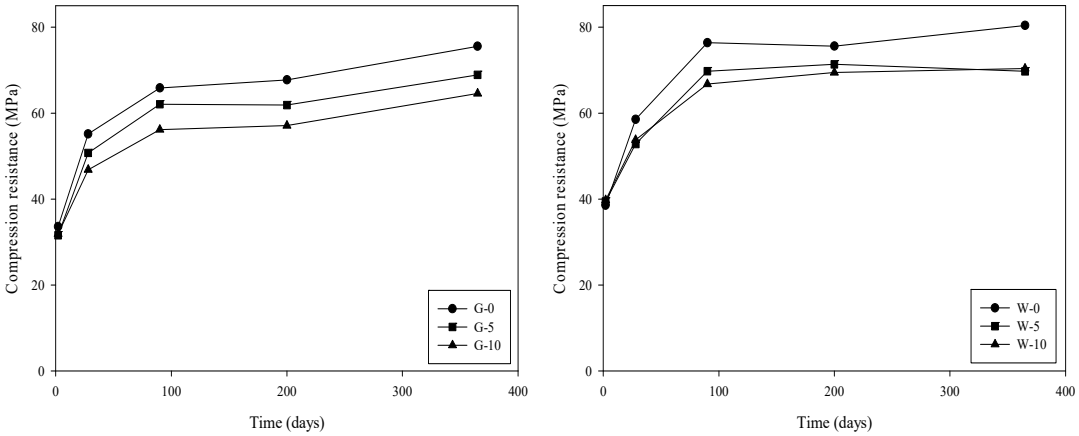

Figure 1. Compression strength. (**a**) G-samples (**b**) W-samples.

Table 2 shows the initial and final setting times for the two untreated cements and for the same two cements with the addition of the photocatalyst. The starting times for the setting of the two cement types were similar and the addition of the photocatalyst had the same effect on both types, namely a significant lowering of this starting time. With the incorporation of 5%wt. of P25, setting commenced approximately 1 h sooner. However, the incorporation of larger quantities of P25 did not result in further significant changes in this respect, with a difference of just 10 minutes between G-5 and G-10. It was not possible to establish a correct study for the W-10, which displayed a high degree of dryness as observed in the consistency study. The mixtures studied all comply with the legislation in force which establishes an initial setting time of ≥ 45 min. The results show that the photocatalyst acts as a setting accelerator. This same behaviour has been observed by other authors [21,22] who incorporated a SiO_2-based photocatalyst in Portland type I cement (manufactured in Taiwan), though with higher proportions of photocatalyst. The size, specific surface area and shape index of the particles of the photocatalyst, whether TiO_2 or SiO_2, contribute to this setting acceleration and to a higher porosity which, as previously mentioned, also results in a reduction in compression strength.

Table 2. Setting times.

Sample	Initial Setting Time	Final Setting Time	Setting Time
W	2 h 51 min	3 h 41 min	50 min
W-5	1 h 52 min	2 h 32 min	40 min
W-10	-	-	-
G	2 h 45 min	4 h 36 min	1 h 51 min
G-5	1 h 52 min	3 h 22 min	1 h 30 min
G-10	1 h 40 min	2 h 30 min	50 min

3.2. Physicochemical Properties

The main species present in the mortars under study were identified by XRD, with no significant differences observed. Figure 2 represents the XRD diffractogram corresponding to G-10, showing the majority species in the sample. Portlandite, sand quartz and the anatase and rutile phases of the photocatalyst were identified [6,23]. The signals corresponding to anatase and rutile were observed in the W-5, W-10, G-5 and G-10, confirming that the TiO_2 maintains its structural integrity in the mortar specimens. The product of portlandite carbonation, calcium carbonate, was not detected in a routine XRD diffractogram.

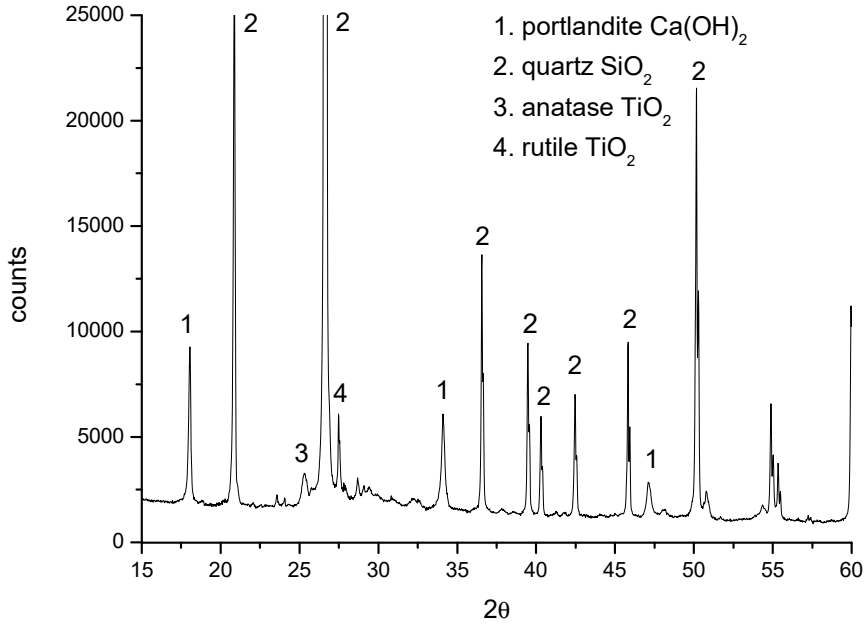

Figure 2. X-ray diffraction (XRD) of G-10.

The degree of hydration and the percentage of portlandite in the mortars were determined from the thermogravimetry analyses. Four thermal regions can be seen in the curve that was obtained (Figure 1). The first region is due to the loss of free and adsorbed water. The second corresponds to decomposition of the calcium hydroxide (portlandite) and the subsequent evaporation of water.

$$Ca(OH)_2 \rightarrow CaO + H_2O \quad (4)$$

The next region corresponds to decomposition of calcium carbonate, which is the result of carbonation of the sample through the reaction of portlandite with carbon dioxide in the air.

$$CaCO_3 \rightarrow CaO + CO_2 \quad (5)$$

Table 3 shows the percentage of hydration and of portlandite in each of the mortars studied. In the case of cement G, it can be seen that both the hydration and portlandite percentages remain practically unaltered with the addition of TiO_2. However, in the case of cement W, both percentages decreased slightly as the amount of photocatalyst increased. This is consistent with the increasing dryness of these samples. The results obtained are similar to those obtained by Chen et al [24], with percentages of around 29–30%. The hydration percentages are around 2.5–3%, similar to values published in other studies [25].

Table 3. Percentages of hydration and portlandite in the studied mortars.

Samples	%Hydration in the Mortar	%Portlandite (%Ch) in the Cement
W	3.31	32.9
W-5	2.96	30.9
W-10	2.47	29.7
G	2.91	29.3
G-5	3.07	29.4
G-10	3.06	30.0

Sample porosity was measured at 28 days. Table 4 shows the microstructural characteristics of the mortars in terms of porosity and mean pore size. An increase in porosity was observed in both cements due to the presence of the photocatalyst, which explains the previously mentioned decrease in strength. Cement G porosity rose from 7.14% to 12.20% and 11.58% for G-5 and G-10, respectively, while cement W porosity rose from 7.26% to 9.39% and 10.12% for W-5 and W-10, respectively, as a result of the presence of the photocatalyst.

Table 4. Characteristics of the microstructure of the mortars.

Samples	Total Porosity (% vol.)	Mean Pore Size (μm)
G	7.14	4.02×10^{-2}
G-5	12.20	4.17×10^{-2}
G-10	11.58	4.20×10^{-2}
W	7.26	3.88×10^{-2}
W-5	9.39	4.55×10^{-2}
W-10	10.12	1.61×10^{-1}

Figure 3 shows pore volume distribution for all the samples. The pore diameter range is the same for all the samples. That is, they all display porosity in the interval 7×10^{-3} to 200 μm. As for pore size distribution, practically no change was observed in the case of cement G when the photocatalyst was present. However, for cement W, a noticeably marked shift to larger pore sizes was observed with W-10. This is confirmed by the mean pore sizes shown in Table 4. These significant changes for the W-10 sample are presumably due its low setting time and lower hydration. In addition, it is possible that TiO_2 nanoparticles beyond approx. 1.5%wt. replacement could agglomerate and cause more voids if care is not taken to ensure good dispersion [26]. Nonetheless, TiO_2 appears to act as an efficient filler in lower additions [9]. In terms of carbonation, no significant influence was found when incorporating P25 in the conventional mortars. No important carbonation was seen at 28 days, despite the detection of the presence of $Ca(OH)_2$ in the thermal analysis. Carbonation was more significant at 365 days, though as the mortars both with and without TiO_2 were affected to the same degree it would appear that the presence of the catalyst has no effect on this property (Figure 4).

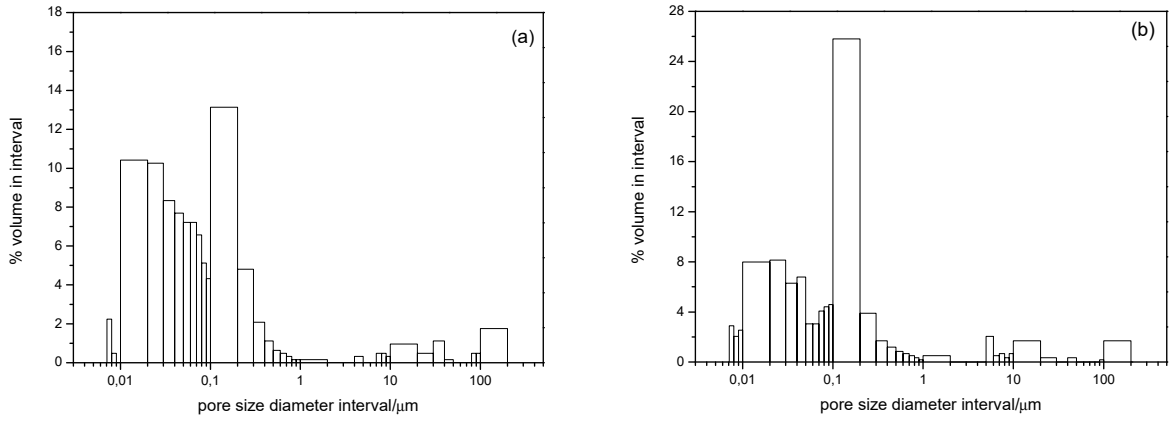

Figure 3. *Cont.*

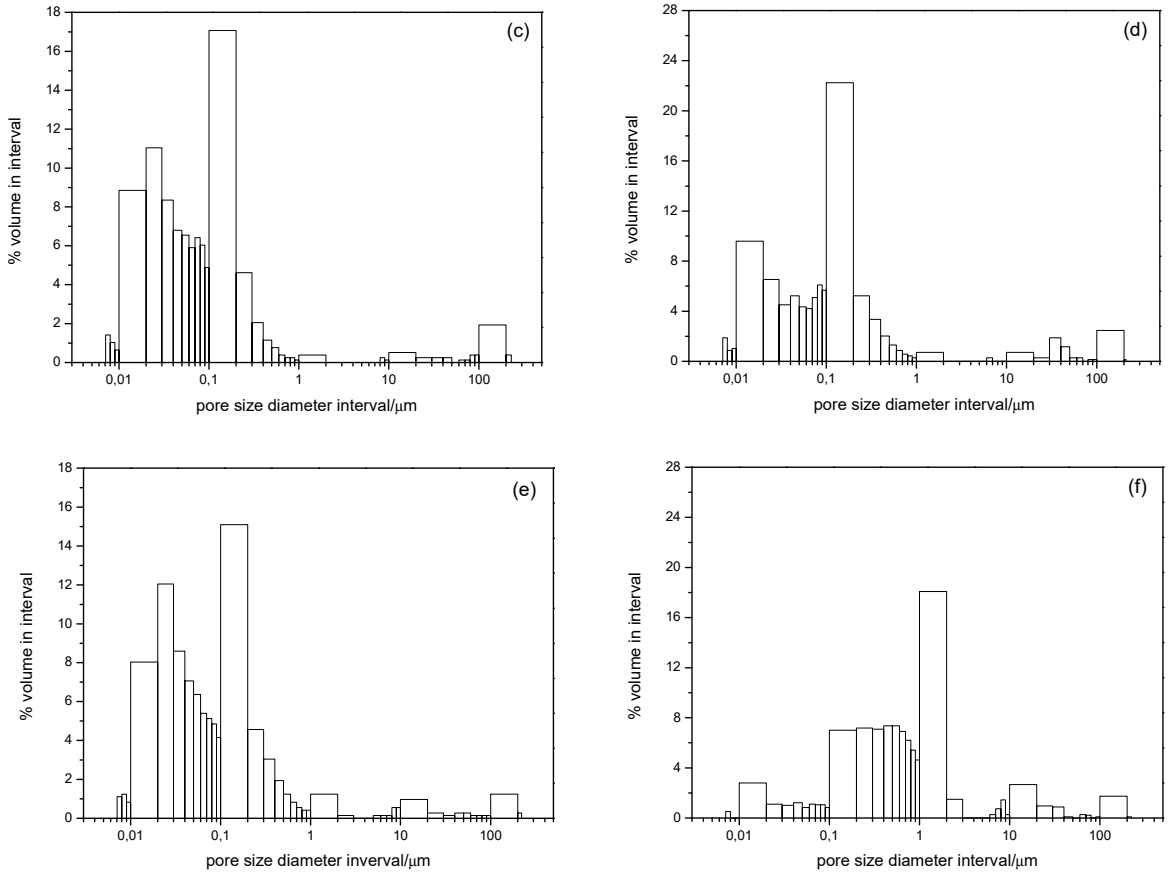

Figure 3. Porosity distribution of the samples: G (**a**), W (**b**), G-5 (**c**), W-5 (**d**), G-10 (**e**) and W-10 (**f**).

Figure 4. Carbonation of W (**a**), W-10 (**b**), G (**c**) and G-10 (**d**) at 365 days.

3.3. Photoactivity

Table 5 shows the NOx percentages removed after 5 h of radiation for the photocatalytic cements with P25 under different humidity conditions (0% and 65% RH). Both mortars without TiO_2 show a little photocatalytic activity. The mortars are able to achieve small photocatalytic efficiencies in the absence of TiO_2 as a result of the hydroxides present in their matrices [27].

Table 5. NOx removed (%) according to different study conditions.

Samples	0% RH	65% RH
G	5.61	11.84
G-5	15.02	14.24
G-10	23.34	20.90
W	0.00	1.53
W-5	9.34	3.57
W-10	12.53	12.98

A slight increase in NOx removal is observed as the amount of photocatalyst present in the mortar samples increases. This trend has also been observed by other authors who used different photocatalysts but with a similar proportion of additive to that used in the present study [23,27,28]. The photoactivities were slightly worse in the presence of humidity due to the competition of water and NOx molecules for active centres on the TiO_2 surface. Higher photoactivity was obtained with cement G, with NOx removal values for G-10 of 23.34% and 20.90% for 0% and 65% RH, respectively. In contrast, the corresponding values for W-10 were only 12.53% and 12.98%. The main compositional difference between the two cements is the higher percentage of Fe_2O_3 in cement G, which could be favouring this higher photocatalytic activity.

In photocatalysis, the effective surface of the photocatalyst is the surface which is in contact with the pollutant as well as that which is exposed to radiation [29]. When incorporating the photocatalyst in the mortar bulk, most of it is inactive for NO oxidation given that photons cannot fall on them. With this in mind, the catalyst was only incorporated into a 1 cm thick surface layer on the specimen to ensure a higher efficiency process. In this way, material requirements can be reduced, making the final product a little more cost effective [30]. This layer was made with and without sand and with catalyst additions of 10%wt. and more, which meant the proportion of water had to be increased to 1.3 due to its adsorption by the catalyst. Nonetheless, the presence of this layer with its different composition to the rest of the specimen did not affect its properties in terms of flexo-traction and compression up to the tested catalyst proportion of 10%wt. For higher catalyst loads, especially in the presence of sand, the thickness of this layer and/or the water addition would need to be optimized [26] (Table 1).

Figure 5 shows the percentage of NOx removed for 0% RH and 65% RH with the incorporation of this layer. When comparing these results with those shown in Table 5, it can be seen that the photocatalytic efficiencies obtained with the photocatalyst incorporated in the surface layer are much higher. This suggests that slightly increasing the water content and working with smaller amounts of mixture allows better dispersion of the TiO_2 in the mixture [26].

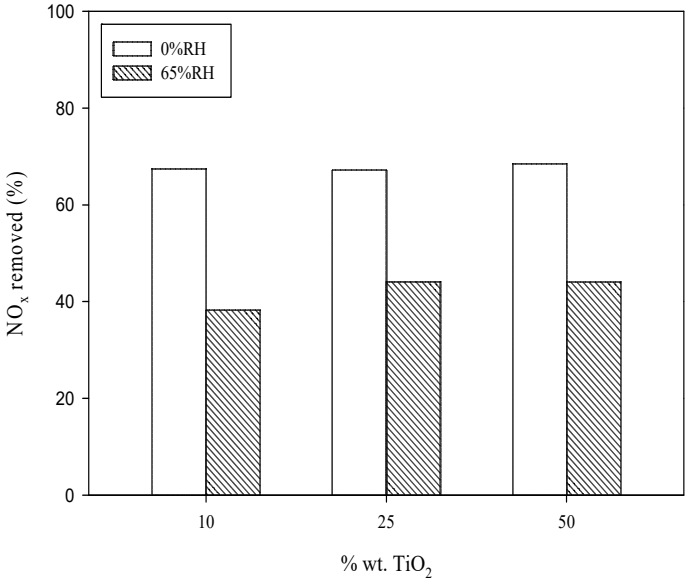

(**a**)

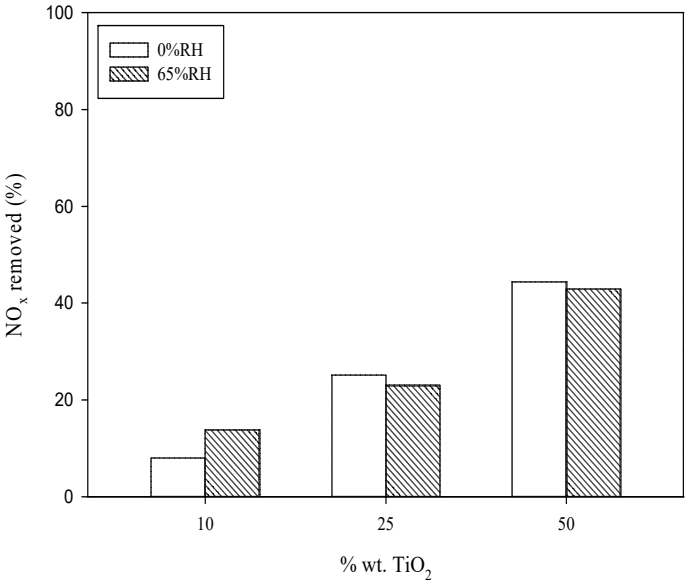

(**b**)

Figure 5. *Cont.*

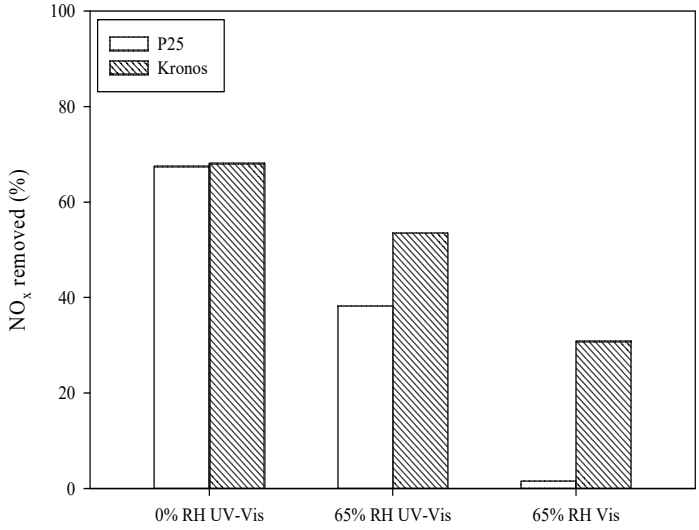

(**c**)

Figure 5. NOx removed with mortars with photoactive surface layer after 28 days: with sand (**a**), without sand (**b**), comparison of P25-Kronos (**c**).

In addition, significant differences can be seen between the two types of surface layer, with and without sand. Photoactivity is higher for the layers which contain sand, regardless of the amount of catalyst. In the absence of humidity, NOx removal rates of 67–68% were obtained, values which remained stable for the 10–50% range of catalyst added to the surface layer. However, without sand, although the amount of removed NOx rose as the amount of catalyst increased, with 50% TiO_2 the elimination rate of NOx was just 44%. This difference may be attributable to the presence of sand allowing greater availability of the TiO_2 and favouring maintenance of its photocatalytic function. Without sand, it is possible that the chemical interaction between the TiO_2 and the cement is even higher [31] and that there is higher aggregation of the TiO_2 nanoparticles [32]. Both circumstances would lead to a decrease in photocatalytic activity, as also observed by Inkyu Rhee et al. [33]. The presence of humidity had a more significant negative effect on the layers with sand, although their activities never fell below those of the layers without sand.

Having observed the feasibility of adding TiO_2 to the mortars, it was decided to determine whether the activity could be improved by testing another semiconductor. For this purpose, the P25 was compared for photoactivity efficiency with Kronos, a more expensive photocatalyst which is active under visible radiation (Figure 5c). It can be seen that, for 0%RH and UV-Vis radiation, both photocatalysts present similar photocatalytic activity, eliminating approximately 68% of NOx. With 65%RH and UV-Vis radiation, Kronos performs better, with 28% more NOx elimination compared to P25. With 65%RH and Vis radiation, Kronos completely outperforms P25, which shows no activity under these study conditions. In this case, Kronos, removes approximately 30% of the NOx in the system. It could therefore be possible to employ a range of photocatalytic mortars. Choosing which one to use would depend on the conditions in which they are required to work and the particular requirements of their intended function.

4. Conclusions

The presence of the photocatalyst confers photocatalytic activity to the mortars. It has been shown that adding the photocatalyst to mortar has no significant effect on its mechanical properties and that it can be used as an additive to accelerate the setting time. Though flexural and compression strength decrease, the values remain above the legally required minimum value of 52.5 MPa. The percentages of hydration and portlandite remain practically unaltered and there is no significant effect on carbonation when incorporating TiO_2 in the mortars. The percentage of removed NOx increases with the addition

of catalyst to the mortar specimens and is negatively affected in the presence of humidity. Incorporating the photocatalyst only in a 1 cm thick surface layer on the specimens enhances the efficiency of the TiO_2 addition as the only active catalyst is that which receives photons. Higher photocatalytic activity is obtained when sand is present in the mixture than when it is not. From a photocatalytic point of view, 10%wt. TiO_2 seems to be the optimum amount. Although there is a reduction in mechanical strengths, the values still comply with the prevailing legislation. Preliminary photoactivity studies with the addition of another commercial photocatalyst, Kronos, showed that it is possible to improve the results obtained with the most widely used catalyst, P25, especially under visible radiation.

Author Contributions: Conceptualization—M.J.H.R., E.P.M., J.M.D.R., O.G.D.; Data curation, Formal analysis, Investigation, Writing—original draft—E.P.M., M.J.H.R. and R.S.; Funding acquisition—J.M.D.R., O.G.D. and E.P.M.; Methodology—M.J.H.R., E.P.M., R.D. and R.S.; Supervision—E.P.M. and J.M.D.R.; Writing, review & editing—all authors.

Funding: Research was funded by the Spanish Ministry of Economy and Competitiveness through the projects IPT-2012-0927-420000 (HORMIFOT) and CTQ2015-64664-C2-2-P (co-funded by the ERDF).

Acknowledgments: M.J. Hernández thanks the University of Las Palmas de Gran Canaria for its funding through their Research Support Programme.

Conflicts of Interest: The authors declare no conflict of interest. The funders had no role in the design of the study; in the collection, analyses or interpretation of data; in the writing of the manuscript or in the decision to publish the results.

References

1. Faraldos, M. *Guía Práctica de la Fotocatálisis Aplicada a Infraestructuras Urbanas*; Congreso Nacional del Medio Ambiente; Asociación Ibérica de Fotocatálisis: Barcelona, Spain, 2012; Available online: http://www.conama2012.conama.org (accessed on 15 May 2016).
2. Chiron, M. Air pollution by automobile exhaust and public health. *Stud. Surf. Sci. Catal.* **1987**, *30*, 1–10.
3. Castellote, M.; Ramírez, A.M.; Saeki, Y.; Beeldens, A.; Motohashi, K.; Ohama, Y. *Application of Titanium Dioxide Photocatalysis to Construction Materials*; Springer: Berlin, Germany, 2011.
4. Ballari, M.M.; Hunger, M.; Hüsken, G.; Brouwers, H.J.H. NO_x photocatalytic degradation employing concrete pavement containing titanium dioxide. *Appl. Catal. B Environ.* **2010**, *95*, 245–254. [CrossRef]
5. Hassan, M.M.; Dylla, H.; Mohammad, L.N.; Rupnow, T. Evaluation of the durability of titanium dioxide photocatalyst coating for concrete pavement. *Constr. Build. Mater.* **2010**, *24*, 1456–1461. [CrossRef]
6. Mendoza, C.; Valle, A.; Castellote, M.; Bahamonde, A.; Faraldos, M. TiO_2 and TiO_2–SiO_2 coated cement: Comparison of mechanic and photocatalytic properties. *Appl. Catal. B Environ.* **2015**, *178*, 155–164. [CrossRef]
7. Chen, J.; Poon, C. Photocatalytic construction and building materials: From fundamentals to applications. *Build. Environ.* **2009**, *44*, 1899–1906. [CrossRef]
8. Lisbona García, L.E. Materiales Fotocatalíticos y Sus Aplicaciones en Construcción. Ph.D. Thesis, Universidad Politécnica de Cataluña, Barcelona, Spain, 25 February 2016.
9. Sadawy, M.M.; Elsharkawy, E.R. Effect of Nano-TiO_2 addition on Mechanical Properties of Concrete and Corrosion Behavior of Reinforcement Bars. *IJERA* **2016**, *6*, 61–65.
10. Folli, A.; Campbell, S.B.; Anderson, J.A.; Macphee, D.E. Role of TiO_2 surface hydration on NO oxidation photo-activity. *Photochem. Photobiol. A Chem.* **2011**, *220*, 85–93. [CrossRef]
11. Bygott, C.E.; Maltby, J.E.; Stratton, J.L.; McIntyre, R. Photocatalytic Coatings for the Construction Industry. In *International RILEM Symposium on Photocatalysis, Environment and Construction Materials—TDP 2007*; Baglioni, P., Casssar, L., Eds.; Rilem: Paris, France, 2007; pp. 251–258.
12. Ângelo, J.; Andrade, L.; Madeira, L.M.; Mendes, A. An overview of photocatalysis phenomena applied to NO_x abatement. *J. Environ. Manag.* **2013**, *129*, 522–539. [CrossRef]
13. Hernández Rodríguez, M.J.; Pulido Melián, E.; González Díaz, O.; Araña, J.; Macías, M.; González Orive, A.; Doña Rodríguez, J.M. Comparison of supported TiO_2 catalysts in the photocatalytic degradation of NO_x. *J. Mol. Catal. A Chem.* **2016**, *413*, 56–66. [CrossRef]
14. Zabek, P.; Eberl, J.; Kisch, H. On the origin of visible light activity in carbon-modified titania. *Photochem. Photobiol. Sci.* **2009**, *8*, 264–269. [CrossRef]

15. Sanchez-Segado, S.; Makanyire, T.; Escudero-Castejon, L.; Hara, Y.; Jha, A. Reclamation of reactive metal oxides from complex minerals using alkali roasting and leaching—An improved approach to process engineering. *Green. Chem.* **2015**, *17*, 2059–2208. [CrossRef]
16. Robotti, M.; Dosta, S.; Fernández-Rodríguez, C.; Hernández-Rodríguez, M.J.; Cano, I.G.; Pulido Melián, E.; Guilemany, J.M. Photocatalytic abatement of NO_x by C-TiO_2/polymer composite coatings obtained by low pressure cold gas spraying. *Appl. Surf. Sci.* **2016**, *362*, 274–280. [CrossRef]
17. Lucas, S.S.; Ferreira, V.M.; Barroso de Aguiar, J.L. Incorporation of titanium dioxide nanoparticles in mortars-Influence of microstructure in the hardened state properties and photocatalytic activity. *Cem. Concr. Res.* **2013**, *43*, 112–120. [CrossRef]
18. Chen, X.; Wu, S.; Zhou, J. Influence of porosity on compressive and tensile strength of cement. *Constr. Build Mater.* **2013**, *40*, 869–874. [CrossRef]
19. Pérez Nicolás, M.; Navarro Blasco, I.; Fernández, J.M.; Álvarez, J.I. The effect of TiO_2 doped photocatalytic nano-additives on the hydration and microstructure of Portland and high alumina cements. *Nanomaterials* **2017**, *7*, 329. [CrossRef]
20. Pipilikaki, P.; Beazi-Katsioti, M. The assessment of porosity and pore size distribution of limestone Portland cement pastes. *Constr. Build. Mater.* **2009**, *23*, 1966–1970. [CrossRef]
21. Kuo, W.T.; Lin, K.L.; Chang, W.C.; Luo, H.L. Effects of nano-materials on properties of waterworks sludge ash cement paste. *J. Ind. Eng. Chem.* **2006**, *12*, 702–709.
22. Nazari, A.; Riahi, S.; Fatemeh Shamekhi, S.; Khademno, A. Improvement the mechanical properties of the cementitious composite by using TiO_2 nanoparticles. *J. Am. Sci.* **2010**, *6*, 98–101.
23. Pérez-Nicolás, M.; Balbuena, J.; Cruz-Yusta, M.; Sánchez, L.; Navarro-Blasco, I.; Fernández, J.M.; Alvarez, J.I. Photocatalytic NO_x abatement by calcium aluminate cements modified with TiO_2: Improved NO_2 conversion. *Cem Concr. Res.* **2015**, *70*, 67–76. [CrossRef]
24. Chen, K.Y.; Hills, C.D.; Tyrer, M.; Slipper, I.; Shen, H.G.; Brough, A. Characterisation of products of tricalcium silicate hydration in the presence of heavy metals. *J. Hazard. Mater.* **2007**, *147*, 817–825. [CrossRef]
25. Pompeu Correa, P. Estudio Mediante Trazadores de la Disolución de Hidratos de Cemento Portland y Sus Implicaciones en la Durabilidad e Impacto Ambiental de los Materiales de Construcción. Ph.D. Thesis, Universitat Politécnica de Catalunya, Bracelona, Spain, July 2010.
26. Andrade Dantas, S.R.; Serafini, R.; de Oliveira Romano, R.C.; Vittorino, F.; Loh, K. Influence of the nano TiO_2 dispersion procedure on fresh and hardened rendering mortar properties. *Constr. Build. Mater.* **2019**, *215*, 544–556. [CrossRef]
27. Cassar, L. Photocatalysis of cementitious materials: Clean buildings and clean air. *MRS Bull.* **2004**, *29*, 328–331. [CrossRef]
28. Shen, S.; Burton, M.; Jobson, B.; Haselbach, L. Pervious concrete with titanium dioxide as a photocatalyst compound for a greener urban road environment. *Constr. Build. Mater.* **2012**, *35*, 874–883. [CrossRef]
29. Paz, Y. Application of TiO_2 photocatalysis for air treatment: Patents' overview. *Appl. Catal. B Environ.* **2010**, *99*, 448–460. [CrossRef]
30. Xie, N. Mechanical and Environmental Resistance of Nanoparticle-Reinforced Pavement Materials. In *Innovative Developments of Advanced Multifunctional Nanocomposites in Civil and Structural Engineering*, 1st ed.; Kenneth Loh, K., Nagarajaiah, S., Eds.; Woodhead Publishing: Sawston, UK, 2016; pp. 217–246.
31. Feng, D.; Xie, N.; Gong, C.; Leng, Z.; Xiao, H.; Li, H.; Shi, X. Portland cement paste modified by TiO_2 nanoparticles: A microstructure perspective. *Ind. Eng. Chem. Res.* **2013**, *52*, 11575–11582. [CrossRef]
32. Folli, A.; Pochard, I.; Nonat, A.; Jakobsen, U.H.; Shepherd, A.M.; Macphee, D.E. Engineering photocatalytic cements: Understanding TiO_2 surface chemistry to control and modulate photocatalytic performances. *J. Am. Ceram. Soc.* **2010**, *93*, 3360–3369. [CrossRef]
33. Rhee, I.; Lee, J.S.; Kim, J.B.; Kim, J.H. Nitrogen oxides mitigation efficiency of cementitious materials incorporated with TiO_2. *Materials* **2018**, *11*, 877. [CrossRef]